Manoeuvring target detection in over-the-horizon radar using adaptive clutter rejection and adaptive chirplet transform

G. Wang, X.-G. Xia, B.T. Root, V.C. Chen, Y. Zhang and M. Amin

Abstract: In over-the-horizon radar (OTHR) systems, the signal-to-clutter ratio (SCR) used for moving target detection is very low. For slowly moving targets such as ships, the SCR is typically from −50 dB to −60 dB and their Doppler frequencies are close to that of the clutter. For manoeuvring targets, such as aircraft and missiles, the Doppler frequencies are time-varying when a long integration time is considered. When a target does not move uniformly, the Fourier transform based target detection techniques, including super-resolution spectrum techniques, may fail to work appropriately. In such situations, the Doppler signatures are time-varying and, therefore, time–frequency analysis techniques can be used for manoeuvring target detection. In addition, clutter rejection is also required for target detection due to the low SCR. The existing adaptive clutter rejection algorithms combine clutter rejection with spectrum analysis methods, which usually assume uniformly moving target (i.e. sinusoidal Doppler signature) models. An adaptive clutter reject algorithm is proposed together with the adaptive chirplet transform technique for manoeuvring target detection in a multipath environment. Simulation results using a simulated manoeuvring target signal with received raw OTHR clutter data show that targets with SCR below −50 dB can be detected by using the proposed algorithm.

1 Introduction

Over-the-horizon radar (OTHR) systems have been widely used to detect and track targets, such as aircraft and surface ships, in wide area surveillance at long ranges [1–5]. The existing OTHR detection and tracking algorithms are based on the assumption that the Doppler frequency of each target is constant or at least approximately constant during each dwell. Targets are detected from amplitude peaks away from the zero frequency. The detection capability of an algorithm depends on the SCR and the Doppler resolution which, in turn, depends on the length of the coherent integration time (CIT). In the existing Fourier transform based techniques for manoeuvring target detection and tracking, there is a trade-off between the CIT length, SCR and the Doppler resolution. For a slowly or uniformly moving target, such as a ship, the Fourier transform based techniques work well, where a long CIT can be used for clutter spread reduction. However, for a fast manoeuvring target, such as a fast boat, aircraft or missile, in Fourier transform based techniques a long CIT cannot be used and, therefore, the Doppler resolution is limited. In such situations, time–frequency analysis becomes an important technique for effective manoeuvring target detection and tracking. Time–frequency analysis methods [6–10] have found wide applications in radar [11–16]. Because the radar return signals from manoeuvring targets have chirp-like characteristics, a new Doppler processing method based on the adaptive chirplet transform (ACT), instead the Fourier transform, is proposed in this paper. With the adaptive chirplet transform technique, the CIT can be substantially extended and, therefore, the Doppler resolution can be improved compared with Fourier transform based techniques.

In an OTHR system, the detection of slow targets is often difficult, due to clutter from the ground or ocean and the low SCR (typically about −50 dB to −60 dB). Therefore, clutter rejection is necessary to improve the target detect capability. The available clutter rejection algorithms include the Fourier transform based adaptive clutter rejection method recently proposed by Root [2] and super-resolution spectrum estimation algorithms, for example [17, 18]. In this paper, an adaptive clutter rejection algorithm is proposed. After clutter rejection, the ACT is then applied to the clutter-mitigated signal, which makes the energy of the manoeuvring targets concentrated. By using the proposed algorithm, the manoeuvring targets can be correctly detected even when the SCR is below −50 dB.

2 OTHR signal model and problem description

In this Section, we first describe the OTHR signal model and conventional OTHR processing for uniformly moving targets, and then the problem of interest in this paper of manoeuvring targets.

IEE Proceedings online no. 20030700

doi: 10.1049/ip-rsn:20030700

Paper first received 23rd December 2002 and in revised form 27th May 2003

G. Wang and X.-G. Xia are with the Department of Electrical and Computer Engineering, University of Delaware Newark, DE 19716, USA

B.T. Root and V.C. Chen are with the Radar Division, Naval Research Laboratory, Washington, DC 20375, USA

Y. Zhang and A. Amin are with the Center for Advanced Communications, Villanova University, Villanova, PA 19085, USA

2.1 OTHR signal model for OTHR processing

After low-pass filtering and sampling, the received signal $s(m,n)$ for a target p with ground range r is (see for example [4, 5])

$$s(m,n) = A_p \exp(j\omega_p m T_c) \exp\left\{ j\left[\omega_p - 2\pi B f\left(\frac{d_p}{c} - T_0\right)\right] n T_s \right\} + \xi_{n,m} \tag{1}$$

where n, m, T_0, ω_p, d_p, f, B, T_c, and $\xi_{n,m}$ are the fast time sample index, chirp pulse index, the minimum delay, Doppler frequency shift, the two-way slant range, waveform repetition frequency, bandwidth of radar, coherent integration time and additive noise, respectively. A_p in (1) is the amplitude of the received signal from the target (source) or clutter p. The power A_p^2 of the signal has the expression as [19, 20]

$$A_p^2 = \frac{P_t G_t}{4\pi R_t^2} \times \frac{\sigma}{4\pi R_r^2} \times A_e$$

where R_t and R_r are the distances (m) of transmitter and receiver of radar to the target, respectively, P_t is the power (W) of antenna with gain G_t, σ is the cross-section (in square metres) of the target and A_e is the effective area of antenna aperture. From (1), we find that the signal part in $s(m,n)$ in terms of index n is a complex sinusoidal signal. It is also a sinusoidal function of index m if the Doppler frequency ω_p does not change with m. In this case, a two-dimensional discrete Fourier transform over m and n provides the range–Doppler surface $S(m',n')$. The received clutter signal is the signal coming from the ground and surface of the sea. The signal of clutter is spread in frequency, it does not just appear in zero frequency. In the real OTH radar, there are two high peaks corresponding to the Bragg lines away from zero frequency, which make target detection more difficult. For a particular OTHR processing algorithm, the target detection capability depends on the SCR. Therefore, in order to improve the target detection performance, one can increase the range, Doppler resolution and/or the SCR. The range resolution

$$\Delta r = \frac{c}{2B}$$

depends on the bandwidth B of radar. However, the Doppler resolution

$$\Delta\omega = \frac{2\pi}{T_c}$$

depends on the CIT T_c, which is chosen at the receiver. Targets and clutter with Doppler differences less than $\Delta\omega$ are located in one Doppler cell. One Doppler cell is divided into k smaller cells and the SCR is then increased by k times if the CIT increases k times. The assumption here is that the target moves uniformly within the CIT interval. This assumption, however, may not hold when the CIT is long.

2.2 Problem description on manoeuvring target detection

For a manoeuvring target, the signal Doppler frequency ω_p in (1), due to the target motion or nonuniform motion of electron density distribution in the ionosphere [17], is no longer constant but time-varying. Consider a moving target with initial velocity v and acceleration a in the direction of slant range. The Doppler frequency ω_p in (1) is

$$\omega_p(t) = \frac{4\pi}{\lambda}(v + at)$$

The Doppler spread is

$$\Delta\omega_p = \frac{4\pi}{\lambda} a T_c$$

and thus, the number of Doppler cells that the target energy spreads over is

$$\frac{\Delta\omega_p}{\Delta\omega} = \frac{2aT_c^2}{\lambda}$$

Therefore, when the target moves uniformly, i.e. $a = 0$, the target energy is always concentrated in a single Doppler cell. It becomes different, however, when the target moves nonuniformly, i.e. $a \neq 0$. As an example, let us assume $2a/\lambda = 1$. In this case, the target energy spreads over T_c^2 Doppler cells. This implies that, if the CIT T_c increases k times, the number of Doppler cells over which the target energy spreads increases k^2 times. Therefore, in this case, the SCR in Doppler reduces k^2 times compared to that in the uniform moving target case. This tells us that, for a manoeuvring target, the CIT increase does not benefit the OTHR target detection if the Fourier transform is used in the Doppler processing. We next want to propose an adaptive chirplet transform (ACT) in the Doppler processing that may take advantage of the long CIT no matter whether the target moves uniformly or not.

3 Chirp signal detection and adaptive chirplet transform

In OTHR, the received signal corresponding to a range cell is typically a multicomponent signal with time-varying frequency signatures corresponding to the multiple targets with different velocities and the clutter. In this Section, we first review the Wigner–Ville distribution (WVD) and Radon–Wigner transform (RWT) for multiple chirp detection. We then describe the adaptive chirplet transform method which is used in the simulation in Section 5.

3.1 Chirp signal detection using Radon–Wigner transform

WVD of a signal $s(t)$ is defined as follows [7, 8]:

$$W_s(t,\omega) = \int_{-\infty}^{\infty} s\left(t + \frac{\tau}{2}\right) s^*\left(t - \frac{\tau}{2}\right) \exp(-j\omega\tau)\, d\tau \tag{2}$$

where variables t and ω represent the time and frequency, respectively. WVD has the highest resolution for a single chirp signal, but its major disadvantage is the presence of artificial cross-terms caused by the quadratic multiplication nature. For a signal containing multiple linear chirps, the desired WVD auto-terms are straight lines in the Wigner plane, while the undesired cross-terms are manifested as the high-frequency oscillating characteristics. To suppress the cross-terms, we consider the Radon–Wigner transform (RWT), which takes advantage of the above oscillating properties by integrating the WVD along lines with different chirp rate and frequency shift combinations. A large part of the WVD cross-terms is cancelled to each other through the integration, and the residual part of the cross-terms can be further reduced in the Radon–Wigner plane by noting the fact that the RWT auto- and cross-terms have different characteristics. Therefore, a proper mask can be applied to the RWT to reduce the cross-terms with minimum distortion to the auto-terms. The WVD with substantially suppressed

cross-terms can be obtained by transforming the masked RWT back to the Wigner plane [21]. It is proved in [21] that the WVD auto-terms after the inverse Radon transform of the masked coefficients are the same as those in the original WVD. These WVD auto-terms are then used to estimate the instantaneous Doppler frequencies of targets. For other instantaneous Doppler frequency estimation methods, see for example [6, 7].

For multicomponent signals with approximately equal magnitudes, RWT filtering in the Radon–Wigner plane is effective. However, when the magnitudes of the signal components are significantly different, the method may not be effective because the cross-terms between stronger signal components may be larger than the auto-terms of weaker components. In this case, a weaker signal may be shaded in the presence of strong cross-terms and can hardly be detected. In OTHR systems, the signal echo from small targets, such as small boats, are often much weaker than that of the clutter, even after clutter cancellation. In this case, the method we introduced above can be used to detect the strongest signal component and then remove it from the original signal. This procedure is repeated until all the signal components are detected.

3.2 Adaptive chirplet transform for high-order time-varying frequency signals

For a long CIT, the received signal from a manoeuvring target is no longer a linear chirp signal. When the time-varying frequency is a higher order polynomial of time, the signal can be expressed as a combination of several linear chirps over different time intervals. Such a signal representation, introduced by Mann and Haykin [15], is called chirplet transform.

The procedure of chirplet decomposition of a signal is first to estimate the chirp rates $\alpha_1, \alpha_2, \ldots, \alpha_{N_0}$ of $s(t)$ over different segments, and the respective chirps

$$u_i(t) = \exp\left\{j\left(\frac{1}{2}\alpha_i t^2\right)\right\}$$

are then constructed. For a given frame $\{h_k(t),\ k \in Z\}$ and N_0 chirp rates, a new chirplet frame $\{h_k(t)\,u_i(t),\ k, i \in Z\}$ is obtained. Based on this chirplet frame $\{h_k(t)\,u_i(t)\}$, $s(t)$ is divided as

$$s(t) = \sum_{i=1}^{N_0}\sum_{k} C_{i,k}\,\varsigma_i\,h_k(t)\,u_i(t) \tag{3}$$

where $C_{i,k} = \langle s(t),\, h'_k(t)\,u_i(t)\rangle$ is the frame decomposition and $\{h'_k(t),\ k \in Z\}$, is the dual frame of $\{h_k(t),\ k \in Z\}$, $\langle \bullet, \bullet \rangle$ represents the inner product, ζ_i are arbitrary weights satisfying

$$\sum_{i=1}^{N_0} \varsigma_i = 1,\ 0 \leqslant \varsigma_i \leqslant 1 \tag{4}$$

For details about (3), see [13]. To have an efficient frame decomposition, $\{h_k(t),\ k \in Z\}$ should include functions with different time and frequency bandwidths and centre (mean) locations. For example, the following modulated Gaussian functions

$$h_k(t) = \left(\frac{\gamma_k}{\pi}\right)^{1/4}\exp\left\{-\gamma_k(t-t_k)^2 + j\left[\phi_k + \frac{\beta_k}{2}(t-t_k)\right]\right\} \tag{5}$$

are usually used, where γ_k, ϕ_k are parameters that control the envelope and phase of the chirplet, and β_k and t_k denote the frequency and time centres, respectively.

Next, we consider how to construct the chirplet frame. Radon–Wigner transform can be used to estimate these chirp rates. For a given signal $s(t)$, chirp rate α_1 is obtained by searching the largest peak in the Radon–Wigner plane after taking the RWT of the signal. We then obtain the chirplet frame $\{h_k(t)u_1(t)\}$ by modulating the frame $\{h_k(t)\}$ in (5) with

$$u_1(t) = \exp\left(j\frac{\alpha_1}{2}t^2\right)$$

We next estimate which element in the modified frame $\{h_k(t)\,u_1(t)\}$ optimally matches the signal $s(t)$ and denote this element as $u_1(t)h_{k_1}(t)$ where

$$h_{k_1}(t) = \arg\min_k\left\{\left\|s(t) - \frac{\langle s(t),\, u_1(t)\,h'_k(t)\rangle}{\|h_k(t)\|}u_1(t)\,h_k(t)\right\|\right\} \tag{6}$$

Define signal $s_1(t)$ as

$$s_1(t) = s(t) - \frac{\langle s(t),\, u_1(t)\,h'_{k_1}(t)\rangle}{\|h_k(t)\|}u_1(t)\,h_{k_1}(t) \tag{7}$$

By repeating the same procedure of $s(t)$ to $s_1(t)$, we obtain the chirp rate α_2 corresponding to the second largest component of $s(t)$. Let

$$u_2(t) = \exp\left(j\frac{\alpha_2}{2}t^2\right)$$

we obtain

$$h_{k_2}(t) = \arg\min_k\left\{\left\|s_1(t) - \frac{\langle s_1(t),\, u_2(t)\,h'_k(t)\rangle u_2(t)\,h_k(t)}{\|h_k(t)\|}\right\|\right\} \tag{8}$$

and

$$s_2(t) = s_1(t) - \frac{\langle s_1(t),\, u_2(t)\,h'_{k_2}(t)\rangle}{\|h_k(t)\|}u_2(t)\,h_{k_2}(t) \tag{9}$$

Repeating the above procedure, all signal components can be obtained, and signal $s(t)$ can be expressed as $s(t) = \sum_i s_i(t)$. Based on the above decomposition, the instantaneous frequencies of all signal components can be obtained and then used for OTHR target detection.

One can see that the search in (6) and (8) is four-dimensional and thus has a high computational complexity. In order to reduce the complexity, a suboptimal adaptive chirplet transform algorithm with two-dimensional search is given in [14] and is summarised as follows:

Step 1: Chirp rate α_1 and frequency ω_1 are estimated by

$$(\alpha_1, \omega_1) = \arg\max_{(\alpha,\omega)}|D_s(\alpha,\omega)| \tag{10}$$

where $D_s(\alpha, \omega)$ is the RWT of $s(t)$.

Step 2: Let $g(t)$ denote a match filter with centre frequency ω_1. Also, denote

$$u_1(t) = \exp\left(j\frac{\alpha_1}{2}t^2\right)$$

and

$$h_1(t) = g(t) \circ (s(t)\,u_1^*(t)) \tag{11}$$

where $\circ$ is the convolution operator.

Step 3: Coefficient $C_{1,1}$ in (3) is obtained as

$$C_{1,1} = \langle s(t),\, h_1(t)\, u_1(t)\rangle = \int s(t)\, h_1^*(t)\, u_1^*(t)\, dt \qquad (12)$$

Step 4: Let

$$s_1(t) = C_{1,1}\, h_1(t)\, u_1(t) \text{ and } y_1(t) = s(t) - s_1(t) \qquad (13)$$

Step 5: Set $s = y_1(t)$.
Step 6: Stop if the energy of $s(t)$ is small enough, otherwise go to step 1.

Other adaptive chirplet transforms can be found in, for example [9].

4 Clutter rejection

In OTHR, clutter is a multicomponent signal with much stronger power than that of the target signal. To achieve effective target detection, clutter rejection is necessary before ACT is applied. A clutter rejection algorithm using adaptive Fourier transform was proposed by Root [2]. There are some other algorithms [18, 22], in which adaptive clutter rejection and maximum likelihood target detection are combined based on the sinusoidal target signal model. In this Section, adaptive clutter rejection algorithms are discussed, which are independent of target detection methods and do not assume any target signal model. After clutter rejection, time–frequency analysis can be used to make the energy of a manoeuvring target focused.

4.1 Adaptive noise cancelling method used for clutter rejection

To effectively suppress the clutter, we notice the fact that the clutter has high space correlation to its neighbouring range cells. The correlation coefficient may be as high as 0.8–0.9 [18, 22]. Therefore, the received signals at neighbouring range cells can be used to estimate the clutter covariance matrix of the current range cell. The idea of an adaptive noise canceller can be used for the underlying OTHR clutter rejection problem. An adaptive noise canceller is a dual-input, closed-loop adaptive feedback system [23], which makes use of the signal $d(n)$ received at the primary sensor and the signal $v_1(n)$ received at a reference sensor. The signal received $d(n)$ at the primary sensor is composed of the interested signal $s(n)$ and additive noise $v_0(n)$, i.e.

$$d(n) = s(n) + v_0(n) \qquad (14)$$

It is assumed that the signal $s(n)$ and noise $v_0(n)$ are uncorrelated to each other, and $v_1(n)$ is correlated to the noise $v_0(n)$ but is uncorrelated to the signal $s(n)$. The reference signal $v_1(n)$ is used to estimated the noise component in $d(n)$

$$y(n) = \sum_{k=0}^{K-1} w_k(n)\, v_1(n-k) \qquad (15)$$

where $w_k(n)$ are the adjustable tap weights of the adaptive filter. The filter output $y(n)$ is subtracted from the primary signal $d(n)$, resulting in the following error signal:

$$e(n) = d(n) - y(n) = s(n) + v_0(n) - y(n) \qquad (16)$$

The error signal is used to adjust the tap weights of the adaptive filter. The error signal $e(n)$ is the overall system output, which contains the desired signal $s(n)$ with the noise suppressed.

In the OTHR target detection, the desired signal is the echo from targets, whereas the undesired signal is clutter and noise. As the OTHR signal is usually processed after beamforming, a reference sensor receiving only the clutter is not available. However, as we mentioned before, the clutter in one range cell has high correlation with that of its neighbouring range cells, whereas the target signals do not. Therefore, the signals received at neighbouring range cells can be used for clutter suppression, resembling the signal received at the reference sensor in an adaptive noise canceller.

4.2 Adaptive clutter rejection algorithm

In this Section, an adaptive signal subspace method is used for clutter rejection. Let $s_c(t)$ be the received signal after range compression in the current interested range cell and $s_{n_1}(t), \ldots, s_{n_N}(t)$ are received signals after range compression from N neighbouring range cells. Define the following signal vectors $\boldsymbol{S}_c$ and $\boldsymbol{S}_i$ constructed for the current and the ith neighbouring range cells from the all M samples over the CIT:

$$\boldsymbol{S}_c = [s_{c_i}(0),\, s_{c_i}(1), \ldots, s_{c_i}(M-1)]^T \qquad (17)$$

$$\boldsymbol{S}_i = [s_{n_i}(0),\, s_{n_i}(1), \ldots, s_{n_i}(M-1)]^T \qquad (18)$$

Then, the covariance matrix of clutter and external noise can be estimated by

$$\boldsymbol{R} = \frac{\sum_{i=1}^{N} |\eta_i|^\gamma \boldsymbol{S}_i \boldsymbol{S}_i^H}{\sum_{i=1}^{N} |\eta_i|^\gamma} \qquad (19)$$

where

$$\eta_i = \frac{\boldsymbol{S}_c^H \boldsymbol{S}_i}{\|\boldsymbol{S}_c\| \|\boldsymbol{S}_i\|} \qquad (20)$$

is the correlation coefficient between the received signal vectors at the current range cell and the ith neighbouring cell, and γ is a positive scalar and typically takes a value between 1 and 2.

The introduction of term $|\eta_i|^\gamma$ in (19) allows the contributions of the neighbouring range cells to be weighted differently depending on their respective correlation coefficients with the current range cell. By doing this, the contributions from less correlated range cells can be effectively eliminated.

The SVD of $\boldsymbol{R}$ can be written as

$$\boldsymbol{R} = \boldsymbol{U}\boldsymbol{V}\boldsymbol{U}^H \qquad (21)$$

where $\boldsymbol{U}$ is a unitary matrix and $\boldsymbol{V}$ is a diagonal matrix. Columns of $\boldsymbol{U}$ are eigenvectors of $\boldsymbol{R}$, and the elements in the diagonal of $\boldsymbol{V}$ are the corresponding eigenvalues. As the clutter is the dominant component in the received signal, the eigenvectors $u_1, u_2, \ldots, u_M$ corresponding to the M largest eigenvalues can be reasonably associated to the clutter. The projection of the received signal to the orthogonal subspace of the clutter

$$\boldsymbol{S}_{proj} = \left(I - \sum_{i=1}^{M} u_{n_i} u_{n_i}^H\right) S_c \qquad (22)$$

results in a clutter-suppressed signal.

In (17), because the number of neighbouring range cells is usually smaller than the dimension of the variance matrix $\boldsymbol{R}$ to be estimated, it is rank deficient. By considering the

existence of thermal noise, the full-rank covariance matrix $\boldsymbol{R}_1$ of clutter and noise can be estimated as

$$\boldsymbol{R}_1 = \boldsymbol{R} + \sigma^2 \boldsymbol{I} \tag{23}$$

where σ^2 is the noise variance, which can be roughly estimated, and $\boldsymbol{I}$ is the identity matrix. Performing singular value decomposition (SVD) of $\boldsymbol{R}_1$ yields

$$\boldsymbol{R}_1 = \boldsymbol{U}_1 \boldsymbol{V}_1 \boldsymbol{U}_1^H = \sum_{i=1}^{N} \lambda_i \tilde{\boldsymbol{u}}_i \tilde{\boldsymbol{u}}_i^H = \sum_{i=1}^{N} \lambda_i P_i \tag{24}$$

where λ_i is the ith largest eigenvalue of $\boldsymbol{R}_1$, $\tilde{\boldsymbol{u}}_i$ is its eigenvector, and $P_i = \tilde{\boldsymbol{u}}_i \tilde{\boldsymbol{u}}_i^H$ is the projection operator to the subspace generated by $\tilde{\boldsymbol{u}}_i$. From (21), we know that more clutter energy distributed in the subspace vector $\tilde{\boldsymbol{u}}_i$ corresponding to a larger eigenvalue λ_i. The following algorithm provides an efficient way to remove strong clutter without any knowledge of signal

$$\boldsymbol{S}_{proj} = \sum_{i=1}^{N} f(\lambda_i) P_i \boldsymbol{S}_c \tag{25}$$

where $f(\lambda_i)$ is a weighting function that takes a smaller value for a larger value of λ_i. In this paper, $f(\lambda_i)$ is chosen as

$$f(\lambda_i) = \frac{1}{\lambda_i} \tag{26}$$

Therefore, the signal vector, after the adaptive clutter rejection, becomes

$$\boldsymbol{S}_{proj} = \sum_{i=1}^{N} f(\lambda_i) P_i \boldsymbol{S}_c = \sum_{i=1}^{N} \frac{1}{\lambda_i} P_i \boldsymbol{S}_c = R_1^{-1} \boldsymbol{S}_c = (R + \sigma^2 I)^{-1} \boldsymbol{S}_c \tag{27}$$

The noise variance estimate σ^2 controls the rejection level against the clutter components.

5 Simulation results

In this Section, the performance of the proposed algorithms for manoeuvring target detection is shown by some simulation results. The signal data coming from manoeuvring targets is generated based on the signal model (1) and then added to the raw OTHR clutter data. The radar working frequency is 20 MHz. There are 54 range cells in the data. The coherent integration time (CIT) is $T_c = 12.3$ s. The velocity and acceleration of targets in the range direction are from 40 m/s and 3 m/s^2, respectively. The signal-to-clutter ratio is about -53.5 dB.

In our simulations, the following steps are implemented. For the received signal, matched filtering and range compression are first implemented in the range direction. Then, the signal subspace clutter rejection algorithm is applied to remove the clutter where $\gamma = 1$ is used. Lastly, ACT is used on the clutter-rejected signal for target detection.

The signal waveforms before and after adaptive signal subspace clutter rejection to the range cell that contains target are shown in Fig. 1*a*. We can see that the clutter energy is removed about 15 dB by using the signal subspace algorithm. The results can also be verified by the results of Fig. 1*b* and Fig. 1*c*, which are the mesh of range–Doppler results to the data before and after clutter rejection by the adaptive subspace clutter rejection algorithm. It is noted that the clutter suppression at edge range cells is not as effective as the other cells because less neighbouring range cells are available for clutter subspace estimation.

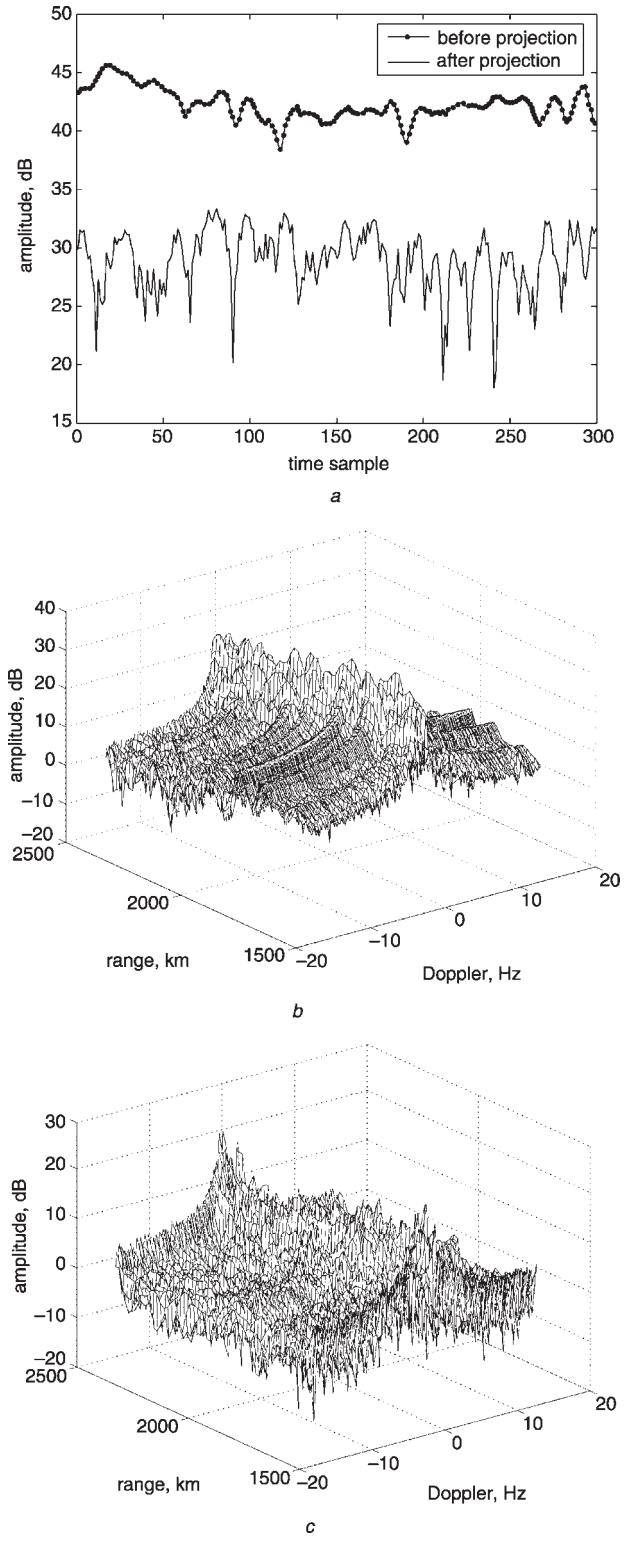

Fig. 1 *Signal amplitude before and after clutter rejection*
a Signal waveforms before and after projection
b FFT range–Doppler before projection
c FFT range–Doppler after projection

The processing results with different methods are shown in Fig. 2. The target cannot be detected from the range–Doppler results obtained by using the Fourier transform on the preclutter rejection data, which is shown in Fig. 2*a*. Because the Fourier transform spreads the target energy of the manoeuvring targets, as shown in Fig. 2*b*, the target is still undetectable even after clutter

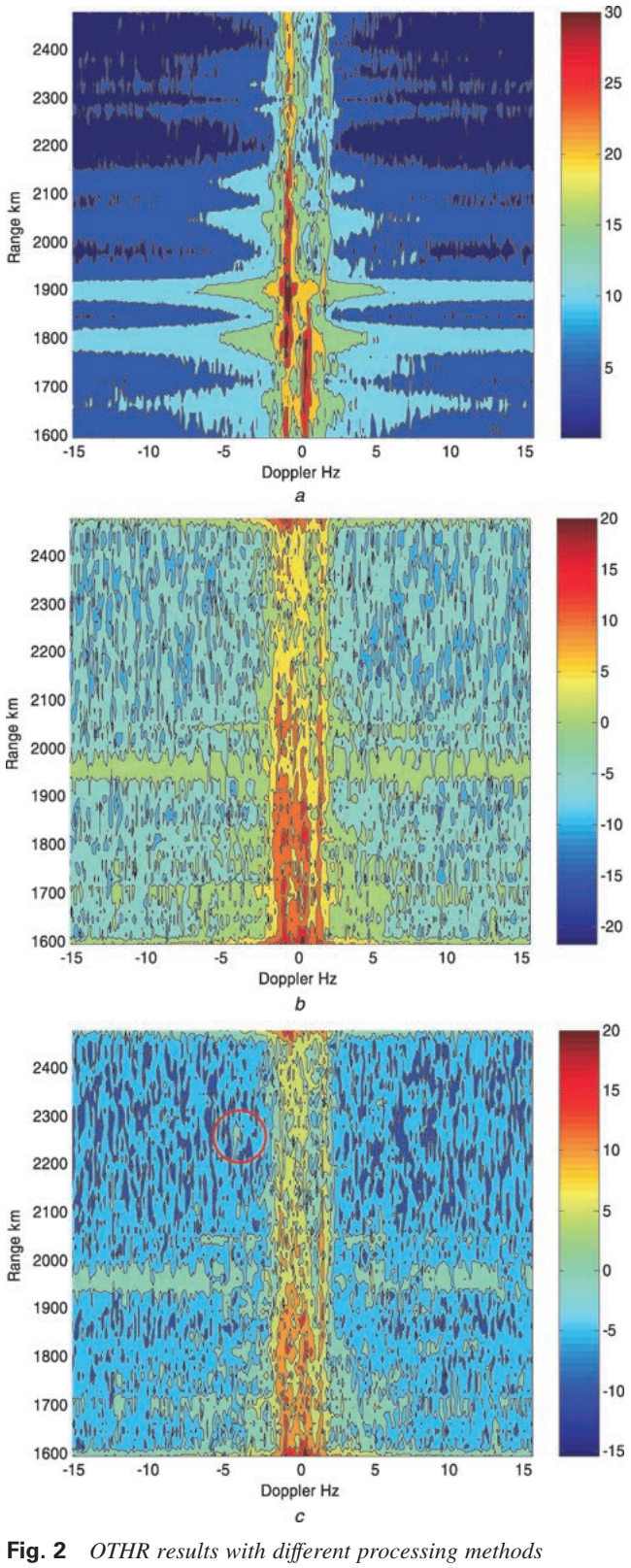

Fig. 2 *OTHR results with different processing methods*

a FFT range–Doppler before projection
b FFT range–Doppler after projection
c ACT range–Doppler after projection

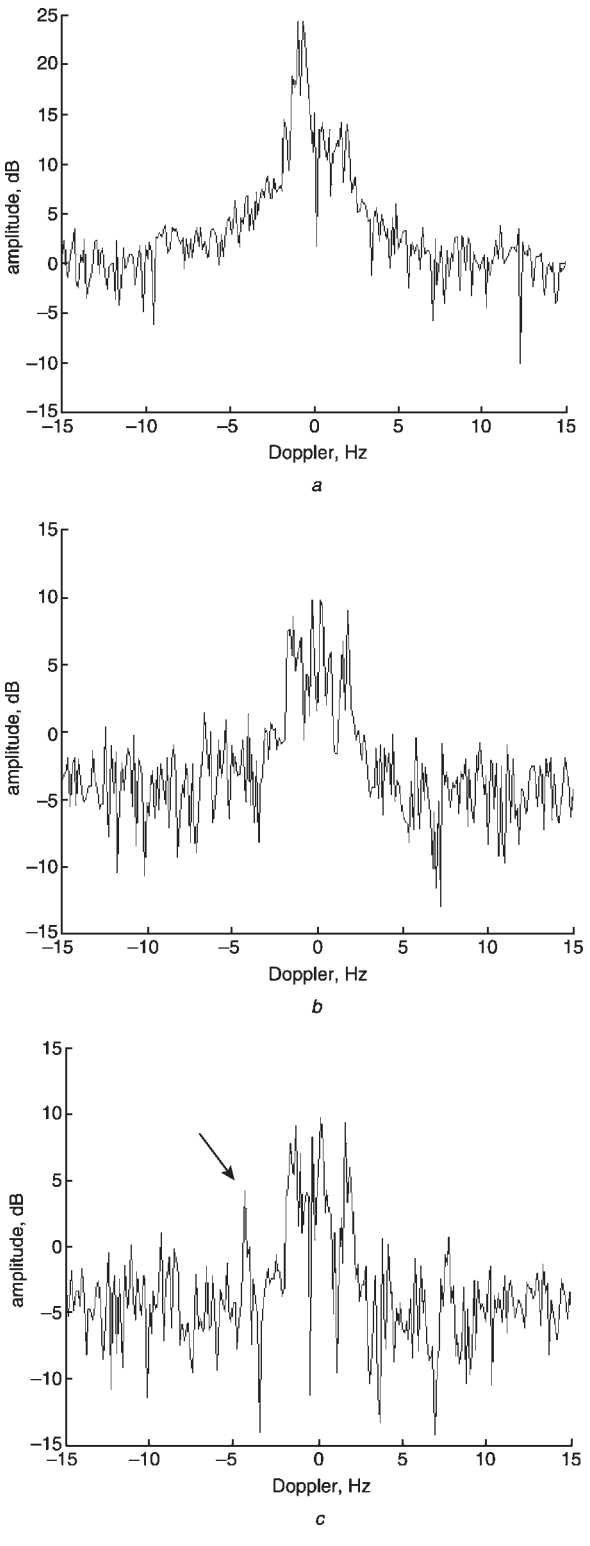

Fig. 3 *Processing results with different methods of the range-containing targets*

a Signal and clutter amplitude after FFT without projection
b Signal and clutter amplitude after FFT and projection
c Signal and clutter amplitude after ACT and projection

rejection and SCR enhancement. Instead of the Fourier transform in Fig. 2*b*, ACT is used in Fig. 2*c*. The target, however, can be easily detected now in Fig. 2*c* at range 2250 km with Doppler about −4 Hz. The amplitudes of the signal in the range cell containing the target are shown in Figs. 3*a*–3*c* for the Fourier transform without clutter rejection, the Fourier transform with clutter rejection and the ACT with clutter rejection, respectively. From Fig. 3*a*, we can see that the clutter amplitude of the main lobe around 0 Hz is about 20 dB higher than that of the sidelobes, including the region around −5 Hz where the target is located. In Fig. 3*b*, although the clutter amplitude of the main lobe is reduced by about 15 dB and the sidelobe is reduced about 5–10 dB, the target still cannot be detected. But in Fig. 3*c*, the target energy is focused. The amplitude of the target signal is about 4 dB higher than that of the clutter in the target's neighbouring frequency bands.

6 Conclusions

In this paper, an adaptive clutter rejection algorithm was proposed for manoeuvring target detection in OTHR systems. This algorithm can reduce clutter energy by about 15–20 dB with negligible distortion to the waveform of the signal returned from manoeuvring targets. An adaptive chirplet transform algorithm was applied to the clutter-mitigated signal for improved Doppler processing. Simulation results showed that the proposed method substantially enhances the target detection ability. Particularly, several simulation examples showed that the proposed method can successfully detect weak target signals where other methods cannot be used directly with adaptive chirplet transform for manoeuvring target detection.

7 Acknowledgments

The work of G. Wang and X.-G. Xia was partially supported by the Office of Naval Research (ONR) under Grant # N00014-0-110059.

8 References

1 Headrick, J.M., and Thomason, J.F.: 'Naval applications of high frequency over-the-horizon radar', *Nav. Eng. J.*, May 1996, **108**, pp. 353–359
2 Root, B.T.: 'HF-over-the-horizon radar ship detection with short dwells using clutter cancellation', *Radio Sci.*, 1998, **33**, (4), pp. 1095–1111
3 McNeal, G.D.: 'The high-frequency environment at the ROTHR Amchitka radar site', *Radio Sci.*, May–June 1995, **30**, pp. 739–746
4 Anderson, R., and Krolik, J.: 'Target localization and track association for over-the-horizon radar with a statistical ionospheric model' Technical Report, Department of Electrical and Computer Engineering, Duke University, 23 July 1999
5 Anderson, R.H., and Krolik, J.L.: 'Over-the horizon radar target location using a hidden Markov model estimated from ionosonde data', *Radio Sci.*, 1998, **33**, (4), pp. 1199–1213
6 Boashash, B.: 'Estimating and interpreting the instantaneous frequency of a signal: Part 1. Fundamentals', *Proc. IEEE*, April 1992, **80**, pp. 519–538
7 Boashash, B.: 'Estimating and interpreting the instantaneous frequency of a signal: Part II. Algorithms and applications', 1992, **80**, pp. 540–568
8 Cohen, L.: 'Time-frequency analysis' (Prentice–Hall, Englewood Cliffs, NJ, 1995)
9 Qian, S., and Chen, D.: 'Joint time-frequency analysis' (Prentice–Hall, Englewood Cliffs, NJ, 1996)
10 Qian, S., Chen, D., and Yin, Q.: 'Adaptive chirplet based signal approximation'. Proc. ICASSP'98, Seattle, WA, USA, 1998
11 Chen, V.C., and Qian, S.: 'Joint time–frequency transform for radar range-Doppler imaging', *IEEE Trans. Aerosp. Electron. Syst.*, 1998, **34**, pp. 486–499
12 Trintinalia, L., and Ling, H.: 'Joint time-frequency transform for radar-Doppler imaging', *IEEE Trans. Aerosp. Electron. Syst.*, May 1998, **34**
13 Chen, V.C., and Miceli, W.J.: 'Time-varying spectral analysis for radar imaging of maneuvering targets', *IEE Proc., Radar Sonar Navig.*, 1998, **145**, (5), pp. 262–268
14 Wang, G., and Bao, Z.: 'Inverse synthetic aperture radar imaging of maneuvering targets based on chirplet decomposition', *Opt. Eng.*, 1999, **39**, (9), pp. 1534–1541
15 Barbarossa, S., and Farina, A.: 'Detection and imaging of moving target with synthetic aperture radar. Part 2: Joint time-frequency analysis and Wigner-Ville distribution', *IEE Proc., Radar Sonar Navig.*, 1992, **139**, pp. 89–97
16 Mann, S., and Haykin, S.: 'The chirplet transform: physical considerations', *IEEE Trans. Signal Process.*, 1995, **43**, pp. 2745–2761
17 Harmanci, K., and Krolik, J.: "Adaptive temporal processing for equatorial spread Doppler clutter suppression'. Proc. IEEE Workshop on Statistical signal and array processing, Pocono, PA, USA, Aug. 2000, pp. 245–249
18 Kraut, S., Harmanci, K., and Krolik, J.: 'Space-time adaptive processing for over-the-horizon spread-Doppler clutter estimation'. Proc. ICASSP'2000, Istanbul, Turkey, June 2000, pp. 3041–3044
19 Skolnik, M.: 'Radar handbook' (McGraw–Hill Publishing Company, 1990, 2nd edn.)
20 Headrick, J., and Skolnik, M.: 'Over-the-horizon radar in the HF band', *Proc. IEEE*, 1974, **62**, (6), pp. 664–673
21 Bao, Z., Wang, G., and Luo, L.: 'Inverse synthetic aperture radar imaging of maneuvering targets', *Opt. Eng.*, 1998, **37**, (5), pp. 1582–1588
22 Nickisch, L.J.: 'Non-uniform motion and extended media effects on the mutual coherence function: an analytic solution for spaced frequency, position, and time', *Radio Sci.*, 1992, **27**, pp. 9–22
23 Haykin, S.: 'Adaptive filter theory' (Prentice-Hall, Englewood Cliffs, NJ, USA, 1996, 3rd edn.)